ACS OMEGA

Open Access

http://pubs.acs.org/journal/acsodf

Article

Green Synthesis of *Withania coagulans* Extract-Mediated Zinc Oxide Nanoparticles as Photocatalysts and Biological Agents

Saima Maher,* Bakht Zamina, Musarat Riaz, Sana Riaz, Noreen Khalid, Muhammad Imran,* Shagufta Fahmid, Hina Ishtiaq, and Shafia Parveen

Cite This: *ACS Omega* 2023, 8, 46715−46727

Read Online

ACCESS | Metrics & More | Article Recommendations

ABSTRACT: Recently, biosynthesized nanoparticles (NPs) have played a vital role as an alternative to physical and chemical methods. Here, a distinctive bioinspired synthesis of zinc oxide nanoparticles (ZnO NPs) has been introduced using leaf extracts of *Withania coagulans* as the reducing agent by using distilled water and methanol. The synthesized catalysts were analyzed through ultraviolet−visible spectroscopy, dynamic light scattering, scanning electron microscopy, Fourier transform infrared, energy-dispersive X-ray analysis, and X-ray diffraction for NP synthesis, morphology, functional group, elemental composition, and peak crystallinity analysis. The phytochemical analysis of 2,2-diphenyl-1-picrylhydrazyl (DPPH), total flavonoid content, total alkaloid content, and total phenolic content of the crude methanolic extract of the plant was also performed, suggesting the greatest potential as the supporting material for ZnO NPs. The NPs were investigated for their catalytic efficiency in the degradation of dyes (rhodamine B dye) and against important human food-borne pathogens (*Staphylococcus aureus*, *Pseudomonas aeruginosa*, and *Escherichia coli*). ZnO NPs exhibited a strong catalytic activity in the degradation of dyes and against bacteria. The results also showed an enhanced activity of ZnO NPs of methanolic extract (ZnO-M) composites compared to zinc oxide of distilled water (ZnO-D). The % age degradation of the dye, K_{app}, and linear relationship were obtained from pseudo-first-order kinetics. The highest reduction rate in 30 and 60 min was observed under sunlight by ZnO-M and ZnO-D, respectively. The rate constant K_{app} for the reduction of the dye was 13.6×10^{-1} min^{-1} and 6.8×10^{-1} min^{-1}, respectively (numerical values). For ZnO-M, $\ln(K_{app}) \approx 0.309$. For ZnO-D, $\ln(K_{app}) \approx -0.385$. These rate constants represent the degradation of the dye in the presence of ZnO-M and ZnO-D catalysts. In addition, NPs were found to be most active against *S. aureus* (18 mm in the case of ZnO-M and 15 mm in the case of ZnO-D) than *P. aeruginosa* and *E. coli*. The results suggested that the prepared ZnO NPs could be used in pharmaceutical industries as well as photocatalysts. ZnO-M had greater control over particle size and morphology, potentially resulting in smaller, more uniform NPs. ZnO-D achieved fine size control but not potentially better than that compared to organic solvents.

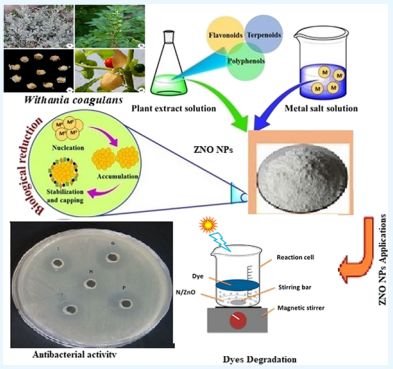

1. INTRODUCTION

In recent years, the field of nanotechnology has experienced remarkable growth and has made significant contributions to a wide range of scientific disciplines. This burgeoning technology has enabled the synthesis of nanoparticles (NPs), leading to the creation of smart materials with unparalleled properties at the nanoscale. The synthesis of functional nanomaterials is a thriving field with immense potential for innovation and real-world applications across various domains. As research in nanotechnology continues to advance, we can expect to see even more breakthroughs and novel applications in the future.[1] Scientists are striving to create well-designed nanomaterials using a range of physical, chemical, and biological processes in light of their incredible applications.[2] There are several uses for nanomaterials in biotechnology, including medication delivery via NPs, biolabeling with fluorescent quantum dots, gene delivery, magnetic separation of biomolecules, drug encapsulation, targeted and controlled drug delivery systems, bioimaging, etc.[3] Nanotechnology's rapid advancement across scientific domains, from medicine to agriculture and materials science, showcases its transformative potential.[4] Meanwhile, promising remarkable benefits, responsible integration, and ethical considerations are vital as we navigate this cutting-edge frontier. Nanotechnology holds the key to addressing critical challenges and shaping the future of scientific innovation. The synthesis of NPs for the manufacturing of new smart materials at the nanoscale with unique properties has rapidly increased in

Received: August 12, 2023
Revised: November 3, 2023
Accepted: November 10, 2023
Published: November 30, 2023

the past few years.[5] NPs can be synthesized by chemical and biological methods. Chemical methods are commonly used to synthesize NPs. These methods involve the chemical reaction of precursor materials to form NPs. Examples include sol−gel synthesis, chemical vapor deposition, and precipitation techniques. One of the most significant concerns with NPs produced by chemical methods is their potential toxicity.[6−8] NPs can behave differently than larger particles of the same material due to their small size. They may enter cells and tissues more easily, leading to adverse effects on living organisms. NPs released into the environment can accumulate and persist, potentially causing harm to ecosystems and wildlife. For instance, certain NPs may be toxic to aquatic organisms and disrupt the natural ecological balance.[9] While NPs have valuable applications in various fields like medicine, electronics, and materials science, they also come with potential side effects and risks, particularly when produced using chemical methods. Understanding and mitigating these risks are essential to ensure the safe and responsible use of NPs in technology and industry. Regulations, ongoing research, and safety measures play crucial roles in managing these risks and ensuring the safe deployment of NPs in society. Green synthesis is considered eco-friendly because it eliminates the need for hazardous chemicals and high-energy processes that are often used in traditional chemical methods.[10] Green synthesis of NPs using plant extracts is an exciting and promising area of research, especially in the field of nanobiotechnology. This method offers environmental sustainability, cost-effectiveness, and nontoxicity, making it attractive for various applications, particularly in biomedicine. However, further research is needed to address challenges and fully harness the potential of green synthesis methods for NP production. In the biomedical field, NPs of metal oxides exhibited auspicious effects against different diseases like anticancer, antimicrobial, cell imaging, etc.[11] Metal oxide NPs, zinc oxide nanoparticles (ZnO NPs), and other metal-based NPs hold great promise in various applications, including antibacterial agents, catalysis, and addressing antibiotic resistance. Their unique properties and mechanisms of action make them valuable tools in scientific research and potentially in medical and industrial fields.[12,13] Metal NPs can target multiple biomolecules in bacteria, compromising their ability to develop resistance. This multifaceted action is a significant advantage in the fight against antibiotic-resistant bacteria.[14−16] Characterizing metal-based NPs using a combination of these techniques provides valuable information about their morphology, physicochemical properties, and electric properties, which are crucial for their *in vivo* activity and the development of safe and effective applications in fields such as medicine and nanotechnology.[17−19] We investigated the effectiveness of green synthesis and the chemical precipitation approach. We have used a pharmacologically important medicinal plant. *Withania coagulans* is widely known as Indian rennet and is one of the most essential plants in Ayurvedic and Unani medicine. This critically imperiled therapeutic plant is a rich natural source of bioactive steroidal lactones known as withanolides.[20] Diabetes can be treated with *W. coagulans*. Aside from ethnobotanical uses, this plant has been linked to antihyperglycemic, anti-inflammatory, antitumor, antimicrobial, hepatoprotective, cardiovascular, immunosuppressive, free radical scavenging, and central nervous system depressant properties.[21] *W. coagulans* offers several advantages for the green synthesis of ZnO NPs, including its effectiveness as a reducing and capping agent, cost-effectiveness, and the absence of harmful chemicals and microbial contamination. These factors make it a promising natural source for NP fabrication, aligning with the growing interest in sustainable and eco-friendly nanotechnology applications. However, it is important to conduct thorough research and experiments to optimize the synthesis process and characterize the properties of the resulting NPs for specific applications.[22] *W. coagulans* methanolic and water fractions were evaluated for bioactivity, such as bioreducing potential for the fabrication of ZnO NPs and antibacterial activities, and the potential influence of dye degradation was also investigated. It has been discovered that *W. coagulans* aqueous and methanolic extracts exhibit strong bioreducing and antibacterial capabilities, and the specific is optimized for practical applications. This provides a low-cost, environmentally benevolent, nontoxic, and efficient source for medicinal and synthetic uses. The *W. coagulans* extract is highly effective in photocatalytic degradation and biological activity.

2. MATERIALS AND METHODOLOGY

2.1. Collection and Preparation of the Plant Extract. Medicinal plants, *W. coagulans*, were collected from Botanic Garden, Department of Botany, Sardar Bahadur Khan Women University, with full permission obtained from an institute. The *W. coagulans* plant material was gently cleaned with tap and distilled water to eliminate dust particles and shade dried to remove residual moisture. Powder was made from dried leaves. Five grams of fine powdered leaves was boiled in 100 mL of double-distilled water for 1 h at 60 °C to make the aqueous extract and filtered through Whatman no. 1 filter paper and kept at 4 °C in a refrigerator. Moreover, methanol was used to make the methanolic extract. The dried powder plant material was soaked in methanol for 3 days and then filtrated. The liquid solution was extracted in a rotary evaporator, and the crude methanolic extract (CME) was kept in a refrigerator.

2.2. Preparation of ZnO NPs by the Green Synthesis Method. A solution of zinc acetate dihydrate ($Zn(CH_3COO)_2{\cdot}2H_2O$) with a concentration of 0.02 M was prepared. To create an aqueous plant extract, 5 g of finely powdered leaves was boiled in 100 mL of double-distilled water for 1 h at 60 °C. The resulting plant extract was filtered through Whatman no. 1 filter paper to remove solid particles and then stored at 4 °C. A solution of 1 M NaOH (sodium hydroxide) was prepared. To synthesize ZnO NPs, 10 mL of the plant extract was mixed with 0.02 M $Zn(CH_3COO)_2{\cdot}2H_2O$ solution. The mixture underwent continuous stirring on a hot plate for 3 h using a magnetic stirrer, resulting in the rapid formation of white precipitates (ZnO NPs). The white precipitates (ZnO NPs) were separated from the solution, likely through filtration using a glass filter, and were then washed repeatedly with distilled water to remove impurities. Further purification was carried out by washing the NPs with ethanol. The purified NPs were finally oven-dried at 100 °C for 1 h to remove any remaining moisture. The thermal stability of the biosynthesized NPs was assessed, and a comparative study was conducted, likely using a similar method with methanol extract. Additionally, ZnO NPs were synthesized using a methanolic extract, which were labeled as ZnO-M. This method represents a green synthesis approach[3] for ZnO NP production, utilizing a plant extract as a reducing and stabilizing agent, potentially resulting in environmentally friendly and unique NPs due to the bioactive compounds

https://doi.org/10.1021/acsomega.3c05947
ACS Omega 2023, 8, 46715−46727

present in the plant extract. ZnO NPs were prepared and labeled as ZnO-M.

2.3. Characterization of the Synthesized ZnO NPs. *W. coagulans* water and methanolic extracts were used for the biosynthesis of ZnO NPs. The synthesized ZnO NPs were characterized through Fourier transform infrared (FTIR) spectroscopy, measuring the absorption of infrared radiation by a sample to identify functional groups and chemical bonds in the material. Ultraviolet−visible (UV−vis) spectroscopy was used to measure the absorption of ultraviolet and visible light by a sample to determine its electronic structure and concentration of absorbing species. Scanning electron microscopy (SEM) was used to produce high-resolution images of the surface of a sample by scanning it with a focused beam of electrons and detecting secondary electrons or backscattered electrons. Energy-dispersive X-ray (EDX) analysis was utilized to determine the elemental composition of a sample by measuring the energy and intensity of X-rays emitted when electrons interact with the sample. Dynamic light scattering (DLS) and X-ray diffraction (XRD) were used to determine the crystalline structure of materials by analyzing the diffraction pattern of X-rays scattered by a crystal lattice. The antimicrobial properties of the biosynthesized NPs were also evaluated against a number of Gram-positive and Gram-negative pathogenic strains, which recommended that these could be used as substitute therapeutics against the drug-resistant microbes in the global emergence of drug resistance.[23−25]

2.4. Phytochemical Analysis. *2.4.1. Total Alkaloid Content.* The alkaloid content was determined by following the Harborne (1973) method with slight modification to determine the total alkaloid content in the plant, and 5 g of plant extracts was added in 10% acetic acid (CH_3COOH) in ethanol, covered, and allowed to stand for 4 h. The mixture was then filtered, and extracts of the plant were then concentrated on a water bath to one-quarter of the original volume. Ammonium hydroxide (NH_4OH) was added for precipitation. The precipitates were collected and washed with dilute ammonium hydroxide and then filtered. Alkaloids were residues that were then dried and weighed.[26,27] This experiment was carried out three times to ensure the accuracy of the results.

2.4.2. Total Phenolic Content and Total Antioxidant Capacity. The total phenolic content and antioxidant capacity were determined with the help of the proposed method by Kamath et al.[28] with little modification. The total amount of phenolic content was determined by the a/c to Folin−Ciocalteu (FC) procedure. The sample (2 mL) (triplicates) was taken into the test tubes and then added 1 mL of FC reagent and 0.8 mL of 7.5% sodium carbonate (Na_2CO_3) and left for half an hour. Gallic acid ($C_7H_6O_5$) was used as the standard. Absorption was made at 750 nm by using a microplate reader. The model of the instrument was UV-1700 SHIMADZU. The calibration curve ($y = 1.5239x - 0.065$; $R^2 = 0.9912$) was obtained, which acted as a positive control. The correlation was observed as significant at 0.05 levels. Analysis of the sample was performed in triplicate. TPC was expressed as gallic acid equivalents (GAE) per milligram extract (GAE/mg).[28]

The total antioxidant capacity of the plant extract was evaluated by the phosphomolybdenum method. The prepared plant extract (2 mL) was taken and then added into 1 mL of reagent solution (28 mM sodium phosphate (NaH_2PO), 0.6 M sulfuric acid (H_2SO_4), and 4 mM ammonium molybdate (NaH_2PO)) in the test tubes. These tubes were capped and incubated in a boiling bath for 90 min at 50 °C. The test tubes were cooled at room temperature; absorption was taken at 695 nm with the help of a spectrophotometer. Ascorbic acid ($C_6H_8O_6$) was used as the standard by taking different concentrations (0.05, 0.2, 0.4, 0.6, and 0.8 mg/mL). The results were expressed as AAE (ascorbic acid equivalent) in milligram per gram of extract.[28]

2.4.3. Total Flavonoid Content. The total flavonoid content was determined by the aluminum chloride ($AlCl_3$) colorimetric method proposed by Suman (2014). Ascorbic acid ($C_6H_8O_6$) was used as the standard. Standard solution of ascorbic acid was made by dissolving 0.25 g in 100 mL of methanol. A series of dilutions were prepared (0.05−0.8 mg/mL) up to 1 mL and added methanol. Similarly, another stock solution was prepared by taking 0.25 mg/g CME dissolved in 100 mL of methanol and a series of dilutions (0.05−0.8 mg/mL) were then made by adding 1 mL of methanol. An amount of 0.6 mL of 2% aluminum chloride stock solution was added in each test tube and covered by aluminum foil and incubated for 60 min at room temperature. The absorbance noted at 420 nm by a microplate. The total flavonoid content of the test sample was calculated from the calibration curve of ascorbic acid ($y = 0.21x - 0.1444$; $R^2 = 0.9966$) and expressed as mg/g AAE.[29] All of the estimations were carried out in triplicate.

2.5. Radical Scavenging Activity—DPPH Assay. The DPPH (2,2-diphenyl-1-picrylhydrazyl) radical coupling assay was calculated following the V.Y.A. Barku methods.[29] The DPPH assay involved the following procedure while determining the antioxidants in the CME. The solutions of the CME of different concentrations (0.05−0.1 mg/mL) were prepared in methanol. Freshly prepared 1 mL of DPPH solution was mixed with 2 mL of all the samples (0.05−0.1 mg/mL). Ascorbic acid ($C_6H_8O_6$) was used as the standard. After the addition of DPPH solution to the test samples, the solutions were kept in the dark place for 30 min. The UV−vis absorbance was calculated to be 517 nm. To measure the absorbance of the control, the plant extract was replaced with methanol, i.e., 1 mL of DPPH, to make the concentration the same, as was taken in the case of test solutions. The absorbance of the blank was recorded and replaced with methanol. The DPPH radical scavenging capacity assay was subtracted from the absorbance of the reaction mixture and expressed as the percent drop-off in the absorbance of the reacting species compared with that of the control. The experiment was carried out in triplicate; the greater radical capturing capability of the CME of *W. coagulans* was indicated by the declined absorbance of the reaction mixture. The ability to capture the DPPH free radical by the CME was measured through the following equation:

$$\text{Percentage of radical capturing activity} = (\text{Abs(control)Abs(sample)})/\text{Abs(control)} \times 100\%$$

2.6. Antibacterial Assay of the Plant Methanolic Extracts. *2.6.1. Test Microorganism.* The antibacterial potential of the plant extract was evaluated using four bacterial strains causing bacterial diseases. The clinical isolates of *Pseudomonas aeruginosa* (ATCC 4853), *Staphylococcus aureus* (ATCC 23235), and *Escherichia coli* (ATCC 25922) were used for antibacterial analysis during this study. These bacterial strains were isolated from different sources such as pus, urine,

https://doi.org/10.1021/acsomega.3c05947
ACS Omega 2023, 8, 46715−46727

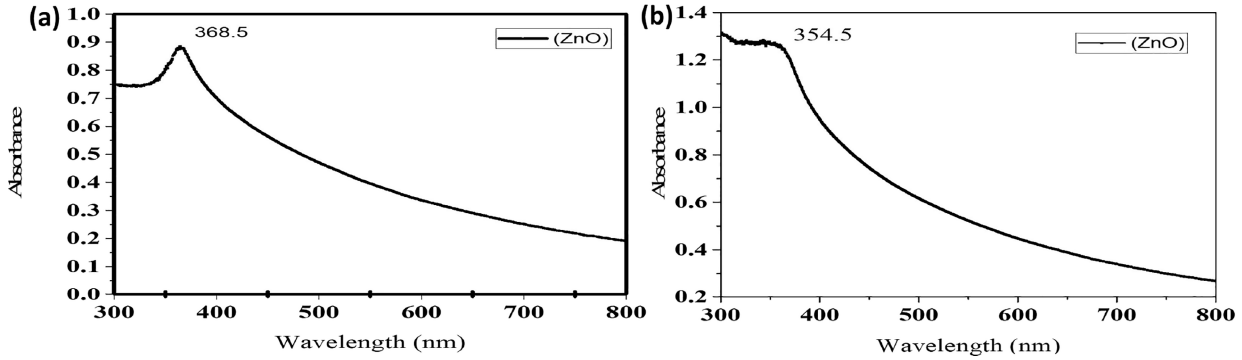

Figure 1. UV−vis spectra of ZnO-D (a) and ZnO-M (b) NPs.

vaginal swab, etc. from the diagnostic laboratory of Aga Khan Hospital, Karachi. Nutrient agar plates were used to preserve the bacterial culture. The temperature for the culture was maintained at 4 °C.

2.6.2. Antibacterial Assay of the Selected Plant Extracts. The antibacterial assay was performed via an agar well diffusion method.[30] All bacterial strains were inoculated into Mueller−Hinton broth for a period of 8 h. The pH was maintained at 7.4 during analysis. Cotton webs were utilized for seeding of isolated organism agar plates. A well of 6 mm was bored with the help of a sterilized metallic borer. DMSO solution was used as a negative control. The 10% DMSO solution was prepared, and 100 μL of this solution along with 1000 μL of test solution was poured into a separate agar plate well. Penicillin G (10U) and ampicillin (10 μg/mL) were used as standard antibiotics, which acted as the positive control against Gram-positive and Gram-negative bacteria, respectively. All plates containing crude plant extract samples (negative control and positive control) were incubated for 24 h at 37 °C. All the samples (plant extracts) were checked in triplicate for each test organism.

2.6.3. Relative Percentage Inhibition. The relative % inhibition was calculated using the formula mentioned below[31] with respect to the standard drug:

$$\text{Relative percentage inhibition of the test extract} = [100 \times (x - y)]/[(z - y)]$$

where x represents the zone of inhibition of the test sample, y represents the total inhibition area of the solvent, and z reflects the inhibition zone of the standard drug.

2.7. Degradation of Rhodamine B Dye. The catalytic efficiency of the prepared ZnO-D and ZnO-M catalysts was carried out by using rhodamine B (RhB) dye and sodium borohydrate ($NaBH_4$) having concentrations 0.05 mm and 0.1 M, respectively. From the prepared solution of dyes, 2.5 mL was taken in the UV−vis spectrophotometer cuvette, followed by the addition of 0.5 mL of freshly prepared $NaBH_4$ solution; in the meantime, by the addition of sodium borohydride, the color change was observed, and the $NaBH_4$ concentration was controlled during dye degradation using the prepared NPs, experiments were conducted with varying NP and $NaBH_4$ concentrations, and the conditions were optimized for maximum efficiency. A control strategy was developed to maintain the desired concentrations during the process. After the addition of 5 mg of catalyst, the solution was put under sunlight and dark conditions to observe the effect of irradiation on the catalytic efficiency. After every 5 min, the color change was monitored by using a UV−vis spectrophotometer to observe the absorbance spectra of the dye before and after the irradiation of sunlight and without any light in dark conditions. In this way, the role of the added different catalysts was investigated on the conversion of colored dye solution to colorless. The regular decrease in the maximum absorbance (λ_{max}) was observed and recorded after every 10 min by using a UV−vis spectrophotometer. The catalytic efficiency of the ZnO catalyst was observed with eqs 1, 2, and 3.

$$\text{Decrease in concentration} = C_t/C_0 \quad (1)$$

$$\text{Removal\%} = (A_0 - A_t)/A_0 \times 100 \quad (2)$$

where C_0 is the initial concentration of the dye, C_t is the concentration at different time intervals, A_0 is the initial absorbance, and A_t is the absorbance at different intervals of time.

The pseudo-first-order kinetics is calculated by

$$\ln\frac{C_t}{C_0} = -k_t \quad (3)$$

2.8. DLS Analysis. The stability of suspensions can be monitored by measuring the zeta potential. Suspensions of ZnO were stable in the neutral pH range. The assessment of the hydrodynamic size and stability of NPs was done in a solution. Specifically, the NPs in question were ZnO NPs, and their size distribution was found to be uniform, ranging from 1.0×10^{03} to 1.0×10^{04} nm. This was determined by using DLS, which provides an average particle size and distribution as well as a polydispersity index (PDI). Before zeta potential measurements, all samples were sonicated for 5 min. Zetasizer Nano ZS used laser Doppler velocimetry to determine electrophoretic mobility. The zeta potential was obtained from the electrophoretic mobility by the Smoluchowski equation. The pH of the suspension was automatically adjusted by an automatic titrator using hydrochloric acid (0.25 and 0.025 mol/L) and sodium hydroxide (0.25 mol/L). The concentrations of additives (SDS, CTAB, and NaCMC) were 5 mmol/L.

3. RESULTS AND DISCUSSION

3.1. Characterization of *W. coagulans*-Mediated NPs. *3.1.1. UV−Vis Spectroscopy.* The UV−vis spectrum of the green synthesized ZnO-D NPs is shown in Figure 1a, which gave an intense blue-shifted maximum absorption peak at 368.5 nm. Maximum absorption peaks exhibited an intensive absorption in the ultraviolet band at about 200−400 nm. The UV−vis spectra showed the formation of the biosynthesized

https://doi.org/10.1021/acsomega.3c05947
ACS Omega 2023, 8, 46715−46727

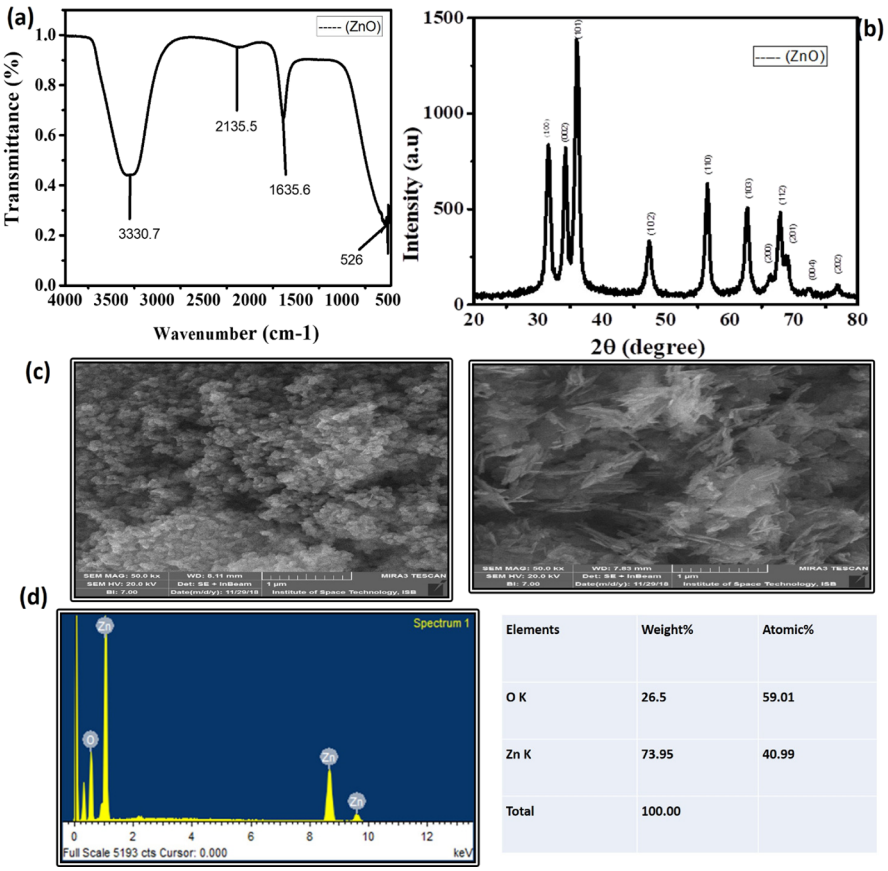

Figure 2. FTIR (a), XRD (b), FESEM (c), and EDX analysis (d) of the biosynthesized ZnO NPs.

ZnO NPs. A sharp peak obtained at 368.5 and 354 nm regions is a great evidence of pure biosynthesized ZnO NPs. Differences in the wavelength of maximum absorption (λ_{max}) and the intensity of absorption peaks of the UV−vis absorption spectra of both catalysts were compared. These differences can indicate variations in the bandgap energy and particle size. The UV−vis spectroscopy results and chemical interactions were clearly evidenced by differences in peak shapes and widths. Wavelength shifts indicate the changes in the electronic structure or environment, with bathochromic shifts (red shifts) indicating lower energy transitions and hypsochromic shifts (blue shifts) indicating higher energy transitions. The ZnO-D showed the peak at 368.5 nm. The ZnO-M (Figure 1b) subjected for UV−vis absorption gave an intense blue-shifted peak at 354.5 nm.

3.1.2. FTIR Spectra of ZnO NPs of W. coagulans. The FTIR of ZnO NPs is shown in Figure 2a. The biomolecules that are present in the plant extract were responsible for the stabilization and reduction of green synthesized ZnO NPs. The FTIR technique showed peaks at 3330.7, 2135.5, 1635.6, and 526 cm^{-1}. An intense and broad peak was observed at 3330.7 cm^{-1} that was due to the stretching vibration of the O−H group. This indicated the presence of the alcohol/phenolic group. The band appearing at 1635.6 cm^{-1} indicated the presence of the carbonyl group (C=O) and primary amine, and the band at 2135.5 cm^{-1} confirmed the presence of nitrile (C≡N) and alkynes (C≡C). The synthesis of pure ZnO was indicated in the FTIR spectra by giving a characteristic peak[20] at 526 cm^{-1}, whereas the same pattern of the FTIR spectrum was observed in ZnO-M NPs.

3.1.3. XRD Analysis of the Biosynthesized ZnO NPs. The size of green synthesized ZnO NPs was confirmed by XRD data (Figure 2b). The XRD data confirmed the crystalline structure of the biosynthesized ZnO NPs. The structure of ZnO NPs was confirmed as hexagonal wurtzite. XRD spectroscopy of ZnO NPs confirmed that ZnO NPs synthesized in their pure phase.[21] In ZnO NPs, the crystalline structure was confirmed by observation at different distinct diffraction peaks at 31.5, 34.2, 36.0, 47.3, 56.4, 62.7, 66.3, 67.8, 68.7, 72.3, and 76.7° in the spectra, which corresponded to the index values of (100), (002), (101), (102), (110), (103), (200), (112), (201), (004), and (202).[22] These Miller index values were compared with JCPDS card no. 36-1451 and concluded that synthesized NPs were a hexagonal wurtzite structure. The same patterns were observed for the ZnO-M NPs.

3.1.4. SEM Analysis. SEM technology was used for identifying the morphology and size of the biosynthesized ZnO NPs. The images of green synthesized ZnO NPs showed that the shape of ZnO NPs was spherical, hexagonal plates, and highly aggregated, with a rough and irregular surface. Meanwhile, ZnO-M showed the flowering structure with an aggregated rough and irregular surface (Figure 2c).

3.1.5. EDX Analysis. EDX analysis confirmed the elemental composition of ZnO NPs. Figure 2 confirms that ZnO NPs are in a pure chemical state. There were two peaks observed between 0 and 2 keV in which one peak was of zinc and other peak was of oxygen and two peaks of the zinc element were observed between 8 and 10 keV. The same EDX result was observed for ZnO-M. The zinc and oxygen weight % (73.95 and 26.5) and atomic % (40.99 and 59.01) result is observed in

https://doi.org/10.1021/acsomega.3c05947
ACS Omega 2023, 8, 46715−46727

Table 1. Detection of Phytochemicals in the Plant Extract of *W. coagulans*

phytochemicals	experiments	observation	result
test for flavonoid	2 mL of extract + few drops of 20% NaOH	intense yellow color + 70% dil HCl; yellow color disappeared	present
test for alkaloids			
(a) Mayer's test	few mL of plant extracts + 2 drops of Mayer's reagent	positive response	present
(b) Wagner's test	few drops of Wagner's reagent added along sides to few mL of plant extracts	reddish brown precipitates	present
test for tannins	2 mL of extract + 10% alcoholic ferric chloride	black color	present
test for phenolic	2 mL of extract + 2 mL of 5% aqueous ferric chloride	blue color	present
test for protein	2 mL of extract + 1 mL of 40% NaOH + few drops of 1% copper sulfate	violet color	present
test for cardiac glycosides	1 mL + 0.5 mL of glacial acetic acid + 3 drops of 1% ferric chloride	brown ring	present
test for carbohydrate	1 mL of extract + few drops of Molisch's reagent + 1 mL con H_2SO_4 at the sides of the tubes, allowed to stand for 2−3 min	red/violet color	present
test for terpenoids	1 mL of extract + 0.5 mL of chloroform + few drops of concentrated H_2SO_4	reddish brown precipitates	present
test for saponins	2 mL of extract + 6 mL of H_2SO_4; shake vigorously	bubbles foam	present
test for detection of diterpenes	water was added to extract + copper acetate solution	no result	absent

Table 1. The result of EDX exhibited that synthesized ZnO NPs were in the chemical state of the selected plant. EDX analysis showed the weight % and atomic % of the zinc and oxygen elements present in Figure 2d.

3.2. Phytochemical Analysis. Secondary metabolites are phytochemicals produced by plants. Various procedures have been conducted for the analysis to establish the existence of secondary metabolites in a selected plant. These analyses are referred to as "phytochemical analysis".

3.2.1. Total Alkaloid Contents. The total alkaloid contents in the CME of the *W. coagulans* plant were calculated to be 0.349 g.

3.2.2. Total Phenolic Contents. The total phenolic content of the methanolic plant extract was estimated by following the method that was mentioned in the experimental part with high phenolic content observed in the methanolic crude extract of *W. coagulans* (Table 2 and Figure 3a). The TPC was expressed in mg/mL of gallic acid equivalents (GAE) per gram of the CME: 3.13 mg of GAE/g extract. The trial was performed in triplicate, and the flavonoid concentration was recorded in μg equiv of gallic acid per milligram extract.

Table 2. Total Phenolic, Flavonoid, and Antioxidant Content Result (Standard)

	total flavonoid content		total phenolic content		total antioxidant content	
s. no.	con. mg/mL	absorbance	con. mg/mL	absorbance	con. mg/mL	absorbance
1	0.05	0.06	0.05	0.01	0.05	0.009
2	0.2	0.29	0.2	0.25	0.2	0.025
3	0.4	0.46	0.4	0.54	0.4	0.043
4	0.6	0.67	0.6	0.75	0.6	0.054
5	0.8	0.92	0.8	0.95	0.8	0.065

3.2.3. Total Flavonoid Contents. The high concentration (0.568 mg/g) of flavonoid was observed in the methanolic crude extract of the *W. coagulans* plant. The results are shown in Table 2 and Figure 3b.

3.2.4. Antioxidant Analysis. The total antioxidant content in the CME of the plant *W. coagulans* was estimated to be 0.061 by the phosphomolybdenum method. The antioxidant calculation (AOC) was expressed in milligrams of AAE per gram of the CME 12.056 mg of AAE/g extract (Table 3 and Figure 4).

3.4.5. DPPH Free Radical Scavenging Activity. The results of antioxidants by the DPPH free radical scavenging assay exhibited a significant conclusion. By increasing the concentration of the CME, the decrease in the absorbance of the DPPH free radical resulted in the selected plant possessing antioxidant activity due to its proton-donating properties (Tables 3 and 4 and Figure 5).

3.5. DLS Analysis. A study found that plant extracts facilitated the synthesis of ZnO NPs with a size distribution of 10 to 120 nm and a maximum size distribution of −90 nm (Figure 6). The "−90 nm" is a specific value that indicates the size of the particles in nanometers. The negative sign indicates that this size is likely an average or median size. The maximum size distribution of −90 nm is based on their DLS analysis; the most common or dominant particle size in the sample is approximately 90 nm. But this size is obtained through the analysis of the intensity of scattered light, and it is often used as a representative value to describe the size of particles in a sample. DLS provides a distribution of particle sizes, and this value represents the peak or central size in that distribution. The actual size distribution may vary, and other parameters, such as the PDI, can provide additional information about the spread or heterogeneity of particle sizes in the sample. While the solution contained particles of uniform size, another broad size distribution peak was observed at 900 nm, which could be due to NP aggregation. It is important to note that capping agents, such as proteins and enzymes present in biological materials, can affect the size of the NPs. The stability of the synthesized ZnO NPs was evaluated using a zeta potential assessment based on the NPs' surface charge. The resulting zeta potential value of −33.4 mV indicated that the synthesized NPs were highly stable in the solution (Figure 6). In a different study, *P. aeruginosa* was used to synthesize ZnO NPs, which were found to have a mean hydrodynamic diameter of 81 nm. This size could potentially be due to NP agglomeration or the hydrodynamic radii of the ZnO NPs, including the solvent layer, which contributes to their stability. This approach utilizes the unique biochemical capabilities of microorganisms to produce NPs. Here is how a bacterial strain like *P. aeruginosa* can be useful in NP synthesis.[32,33] The Smoluchowski equation is used to estimate the zeta potential (ζ-potential) of colloidal particles in a fluid medium. It relates the

https://doi.org/10.1021/acsomega.3c05947
ACS Omega 2023, 8, 46715−46727

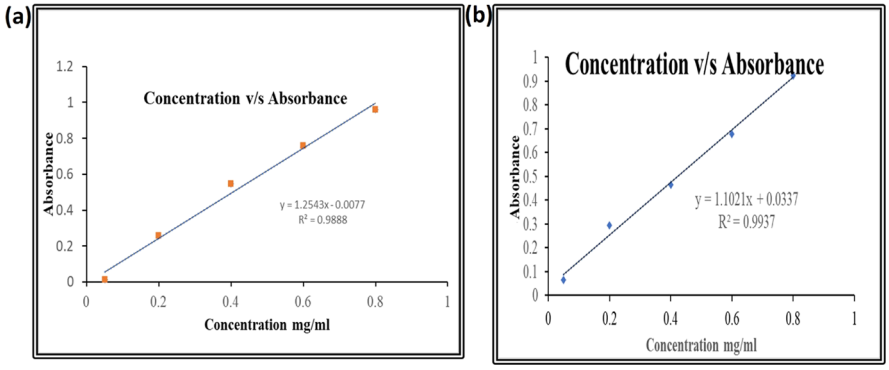

Figure 3. (a) Plant extract absorbance of 0.617 and linear graph of the total phenolic content calculation. (b) Plant extract absorbance of 0.568 and linear graph of the TFC calculation.

Table 3. Antioxidant Activity of Plant Extracts of *W. coagulans*

s. no.	concentration (mg/mL)	abs of blank	abs of test	net abs	abs of control	antioxidant activity
1	0.05	0.012	0.711	0.699	0.8789	20.46876778
2	0.2	0.023	0.521	0.498	0.8789	43.33826374
3	0.4	0.081	0.436	0.355	0.8789	59.60860166
4	0.6	0.112	0.338	0.226	0.8789	74.28603937
5	0.8	0.145	0.257	0.112	0.8789	87.25679827

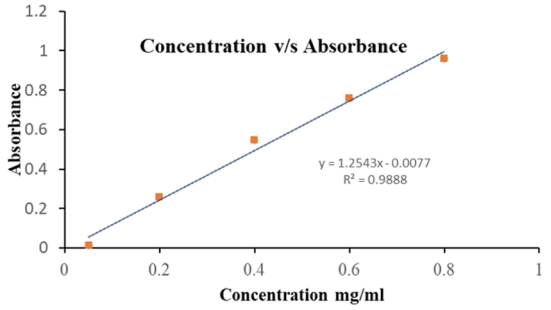

Figure 4. Plant extract absorbance of 0.061 and linear graph calculation.

Table 4. Antioxidant Standard Used[a]

s. no.	concentration (mg/mL)	abs of standard	abs of control	antioxidant activity
1	0.05	0.014	0.8789	98.40709978
2	0.2	0.011	0.8789	98.74843554
3	0.4	0.009	0.8789	98.97599272
4	0.6	0.007	0.8789	99.20354989
5	0.8	0.004	0.8789	99.54488565

[a]Absorbance of control = 0.8789.

electrophoretic mobility (μ) of the particles to the zeta potential with eq 4:

$$[\mu = \{\varepsilon\zeta\eta\}\{\eta 0\}] \quad (4)$$

where μ is the electrophoretic mobility of the particles (measured in $cm^2/V{\cdot}s$ or $\mu m/s{\cdot}V$); ε is the permittivity of the medium (measured in F/m or C/V·m); ζ is the zeta potential of the particles (measured in V); η is the dynamic viscosity of the medium (measured in Pa·s or $N{\cdot}s/m^2$); and $\eta 0$ is the viscosity of the pure solvent (measured in Pa·s or $N{\cdot}s/m^2$).

Overall, this explanation provides insight into the characterization of ZnO NPs' size and stability, highlighting the potential effects of capping agents and different synthesis methods on their properties.

3.6. Antibacterial Activity. Antibacterial activities of ZnO-M showed greater inhibition zones against the following pathogenic bacteria (*S. aureus* and *P. aeruginosa*) than ZnO-D (Table 5). Meanwhile, the CME showed less inhibition zones than ZnO NPs. Additionally, ZnO NPs have the capacity to inhibit the growth of ciprofloxacin-resistant bacteria considerably. There was a direct relationship between the inhibitory effect of ZnO NPs against both standard and resistant bacteria. The highest inhibition of resistant bacteria was shown at 18 mm of ZnO NPs. An NP inhibited the growth of both isolated resistant bacteria by about 15 mm. Moreover, the NP effects in the growth of isolated bacteria are greater than the standard. These results are well-concordant with those of other studies. Additional research has shown that ZnO NPs with a size of 30 nm and a concentration of 6 mM can inhibit the spread of methicillin-resistant *S. aureus* (MRSA), *E. coli*, and several other bacteria.[34] Our results express the effectiveness of ZnO NPs on both standard and isolated *P. aeruginosa* at 18 and 15 mm. Several researchers have investigated various mechanisms of nano-ZnO's antibacterial action.[35] According to certain findings, NPs are more efficient against Gram-positive bacteria than Gram-negative bacteria.[36,37] ZnO NPs exhibit antibacterial activity against both Gram-negative and Gram-positive bacteria. They are generally more effective against Gram-negative bacteria like *E. coli* and *P. aeruginosa* due to differences in the cell wall structure.[38] The NPs disrupt bacterial cell membranes, leading to cell damage and death. But the effectiveness can vary based on the NP size, concentration, and specific bacterial strains. Studies often rely on MIC values and growth inhibition assays to provide experimental evidence for ZnO NP antibacterial activity against specific strains. However, our findings suggested that ZnO NPs have beneficial effects on the bacteria *P. aeruginosa* and *S. aureus*.[39] Ciprofloxacin was chosen as a standard (positive control) since it is not as active as ZnO NPs. As a consequence, ZnO-M demonstrated a strong antibacterial activity. This study

https://doi.org/10.1021/acsomega.3c05947
ACS Omega 2023, 8, 46715−46727

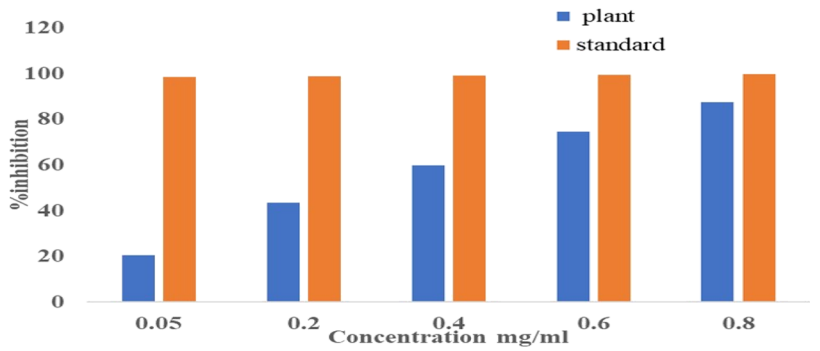

Figure 5. Comparison of % DPPH radical scavenging activity.

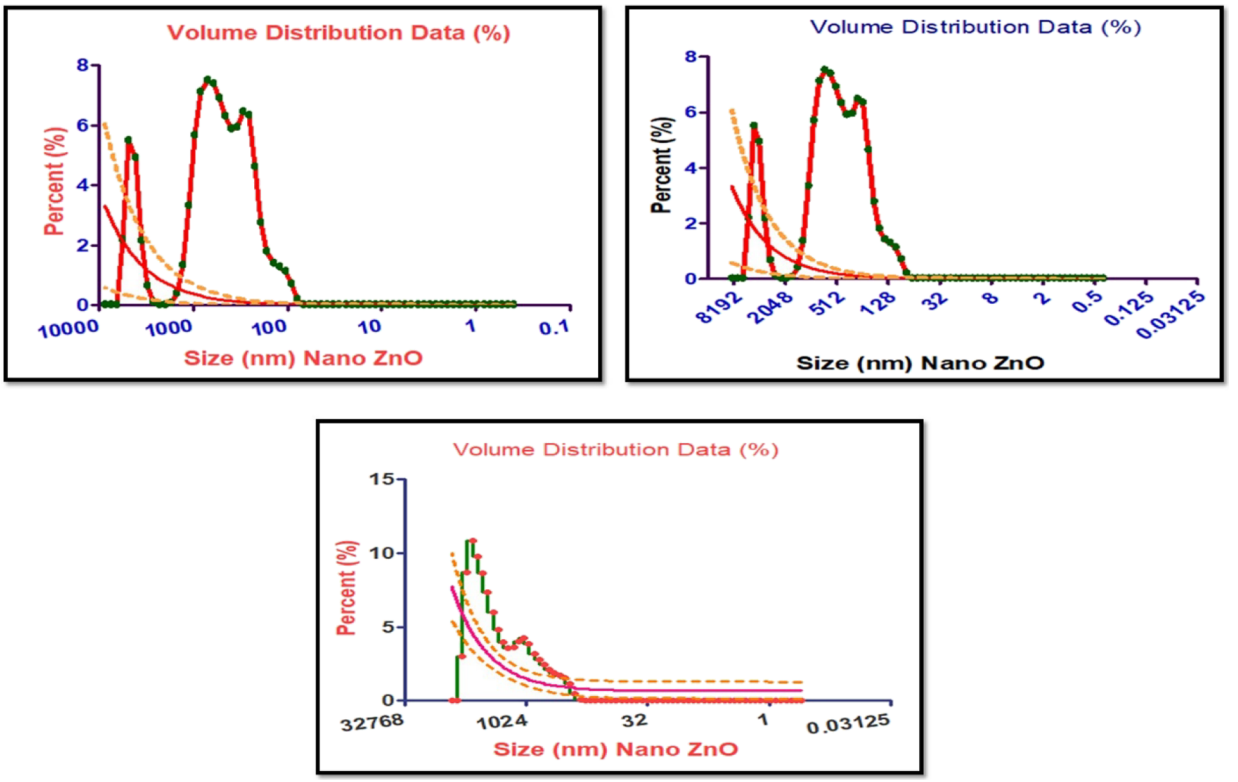

Figure 6. DLS analysis of ZnO NPs.

Table 5. Antibacterial Activity Results of ZnO NPs

	zone of inhibition (mm)			standard
samples	*S. aureus*	*P. aeruginosa*	*E. coli*	ciprofloxacin
ZnO-M	18 mm	13 mm		12 mm
ZnO-D	15 mm	12 mm		10 mm
CME (ZnO-D)	10 mm	11 mm		11 mm
CME (ZnO-M)	9 mm	10 mm		9 mm

indicates that ZnO NPs exhibit antibacterial activity against both negative and positive bacterial strains. This result aligns with previous research in the field that has demonstrated the broad-spectrum antibacterial properties of ZnO NPs. Our findings have reported similar trends in the antibacterial activity of ZnO NPs. These studies have consistently demonstrated the superior antibacterial efficacy of ZnO NPs against specific bacterial strains due to factors such as particle size, surface charge, and release of reactive oxygen species (ROS) upon exposure to bacteria. Our research provides evidence of the antibacterial activity of ZnO NPs against both negative and positive bacterial strains, with a stronger effect observed against the selected strain. We have referenced relevant literature to support our findings and will ensure that this information is appropriately presented in the manuscript to offer a clear and evidence-based explanation.

3.7. Mechanism of ZnO NPs against All Bacterial Strains. ZnO NPs possess powerful antibacterial properties. They work by generating ROS upon contact with water, which damage bacterial cell components (Figure 7). Additionally, ZnO NPs disrupt bacterial cell membranes, leading to the leakage of cellular contents and cell death. They can also enter bacterial cells, causing internal damage to essential processes. Furthermore, ZnO NPs interact with bacterial DNA and proteins, leading to DNA damage and protein denaturation, ultimately inhibiting bacterial growth and causing cell death.

3.8. Degradation of Dyes. *3.8.1. Degradation of RhB Dye.* Recently, water contamination due to industrial revolution becomes a serious issue to the community health.[40]

https://doi.org/10.1021/acsomega.3c05947
ACS Omega 2023, 8, 46715−46727

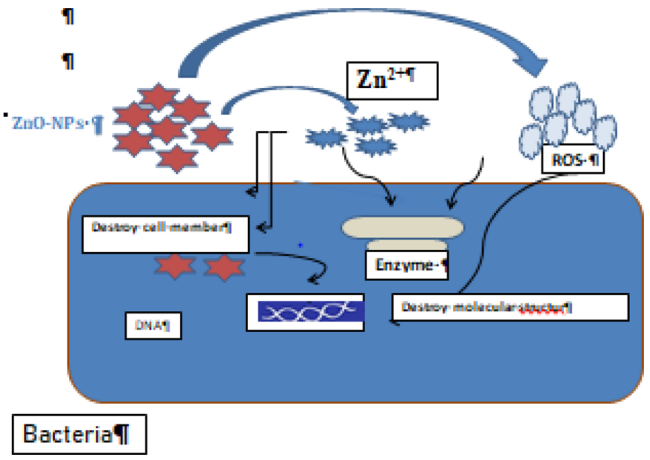

Figure 7. Mechanism of ZnO NPs against all bacterial strains.

Various contaminants such as biodegradable dump waste, heavy metals, dyes, carcinogenic chemicals, and pharmaceutical products are discharged into water bodies. Dye industries discharged the waste effluents directly into water bodies without any proper treatment,[42] which are harmful to the aquatic system, block the photosynthetic activity of plants, and disturb the natural equilibrium process by aquatic diversity reduction. The textile dye RhB 9-(2-carboxyphenyl)-3,6-bis(diethylamino)xanthylium chloride is used as a colorant in drug and cosmetic preparations.[41] It is mostly used as a dyeing reagent in the cell fluorescence, in the study of water pollution used as a tracing agent, and as a colorant in dyeing fabrics, glass, leather, herbicide, and sprays. RhB has toxic effects on health, if ingested.[42] Its chronic carcinogenicity and neuro-toxicity have been proven experimentally. Thus, due to their toxic health effects, the development of a new method for the degradation of RhB is of great significance. In this study, reduction of RhB was carried out by the use of ZnO NPs prepared in deionized water and methanol. A degradation study was carried out under sunlight and dark by using a UV−vis spectrophotometer. The RhB UV−vis spectra showed a strong absorption peak at 556 nm and a small peak at 275 nm.[43] The peak at 557 nm was used to observe degradation, which starts decreasing after the addition of the catalyst. The decrease in the peak intensity was recorded continuously with a time interval of 10 min, as shown in Figures 7 and 8. The peak maxima at 557 nm decreased gradually and a new peak at 255 nm appeared after a short time in the presence of the catalyst showing RhB reduction. The decrease in the peak intensity was continuously recorded with a specific time interval, typically expressed in minutes or seconds, to track changes in the system over time. The time interval helps capture the kinetics of the process. Thus, the catalyst causes the de-ethylation process of RhB at the $-N(C_2H_5)_2$ site by producing aromatic amine *N*-de-ethylated compounds. Figures 8 and 9 show the successful degradation of the dye in the presence of both catalysts. However, ZnO-M was proved more active as compared to ZnO-D produced in water, causing a complete degradation in a short time (Figures 8 and 9). To observe the effect of light on the photocatalytic activity process, RhB removal was investigated by exposing the dye sample under dark and sunlight. RB degradation showed that under dark conditions, the % removal of RhB was less as compared to sunlight by both catalysts. This significant RhB dye degradation in the presence of sunlight obviously showed the role of ZnO as a photocatalyst.[44,45] Furthermore, the degradation reaction showed pseudo-first-order kinetics showing a straight line with respect to the dye by using eq 3. Here, the ZnO-M catalyst showed the highest % reduction and decrease in the initial concentration of RhB with the highest rate constant value within a minimum time as compared to ZnO-D (Figures 8−12 and Tables 6 and 7). The larger removal percentage of ZnO-M (zinc oxide nanoparticles-monodisperse) compared to ZnO-D (zinc oxide nanoparticles-dispersed) can be attributed to factors such as a smaller and more uniform particle size, better dispersion, increased reactivity, surface chemistry, kinetics, agitation, and the nature of contaminants. These factors influence the NPs' ability to interact with and remove specific substances in various applications. The highest reduction rate within 30 and 60 min was observed under sunlight by ZnO-M and ZnO-D, respectively. The rate constant K_{app} for the reduction of the dye was 13.6×10^{-1} min^{-1} and 6.8×10^{-1} min^{-1}, respectively (numerical values). For ZnO-M, $\ln(K_{app}) \approx$

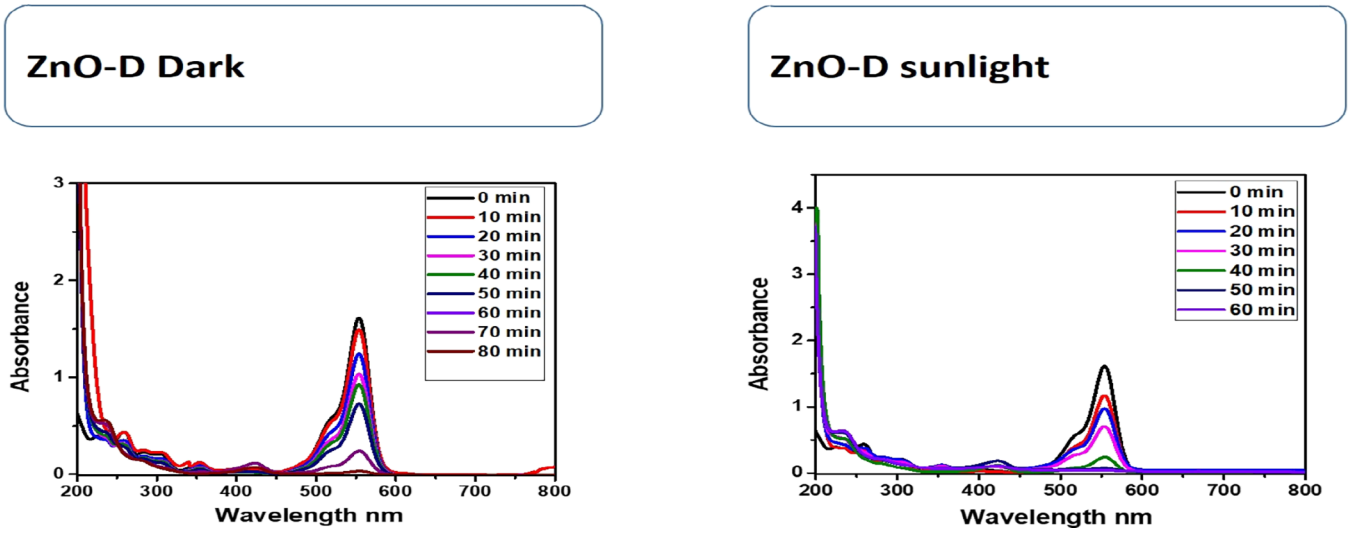

Figure 8. UV−vis spectra of the reduction of RhB dye by ZNO-D under dark conditions and under sunlight.

https://doi.org/10.1021/acsomega.3c05947
ACS Omega 2023, 8, 46715−46727

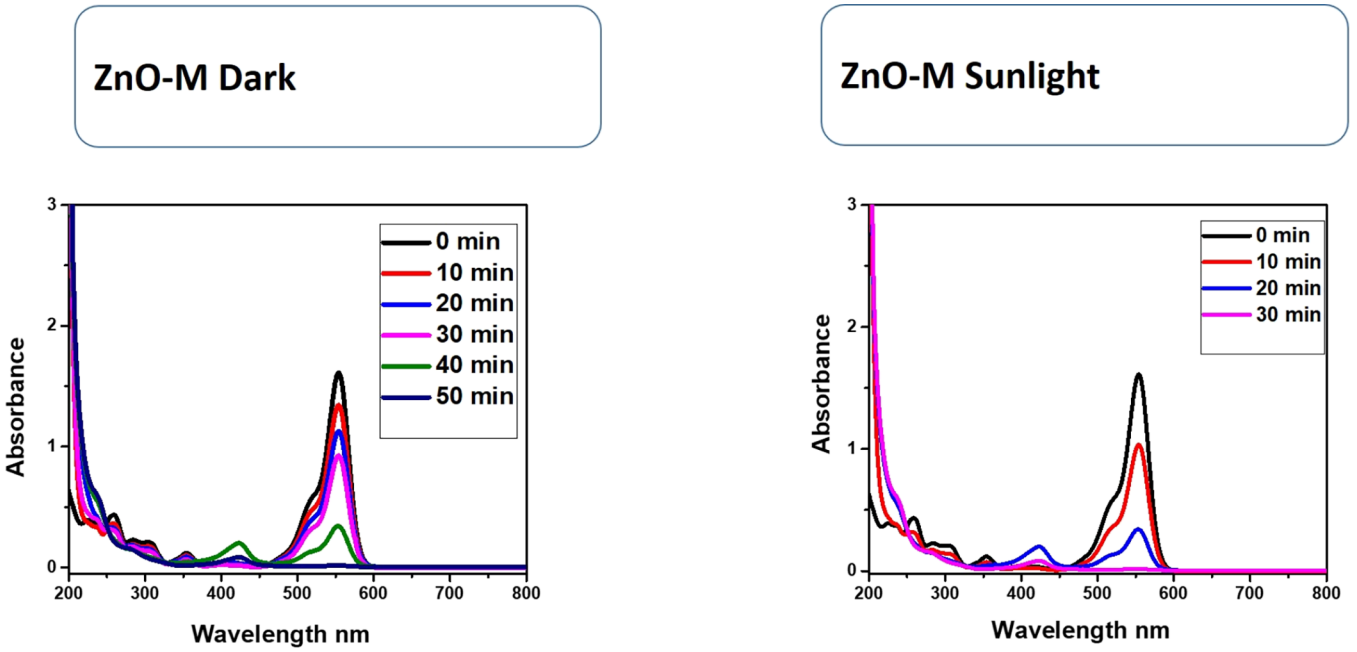

Figure 9. UV−vis spectra of the reduction of RhB dye by ZnO-M under dark conditions and under sunlight.

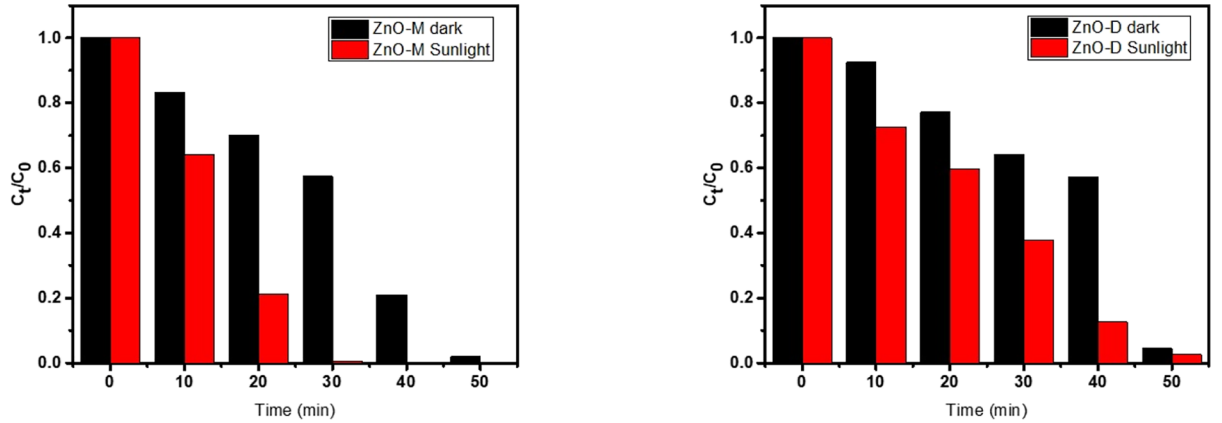

Figure 10. Results of C_t/C_0 for the reduction of RhB dye by ZnO-M under dark/sunlight conditions and ZnO-D under dark/sunlight conditions.

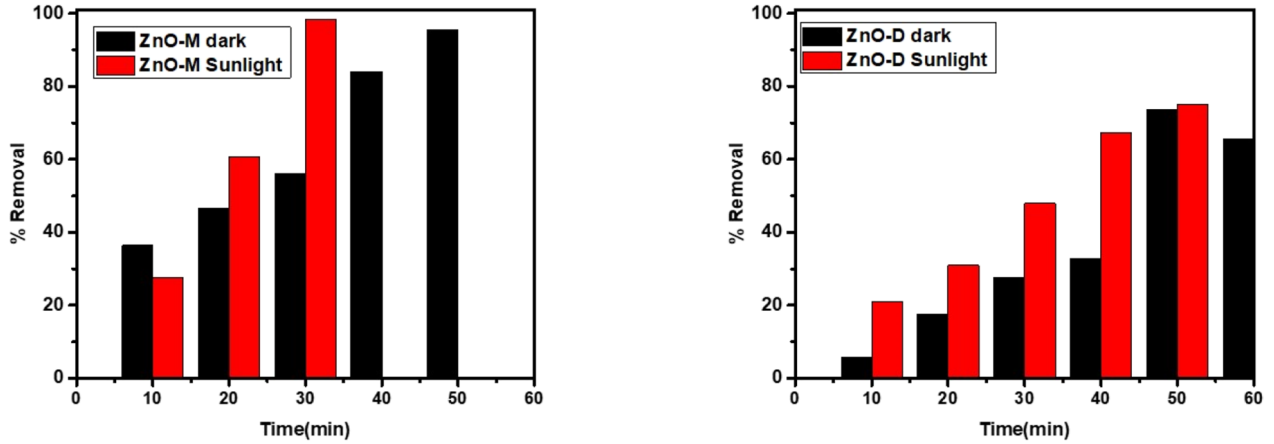

Figure 11. Results of removal (%) for the reduction of RhB dye by ZnO-M under dark/sunlight conditions and ZnO-D under dark/sunlight conditions.

0.309. For ZnO-D, $\ln(K_{app}) \approx -0.385$. These rate constants represent the degradation of the dye in the presence of ZnO-M and ZnO-D catalysts. The reduction of RhB dye by ZnO-D or ZnO-M is more effective under sunlight due to photon-

https://doi.org/10.1021/acsomega.3c05947
ACS Omega 2023, 8, 46715−46727

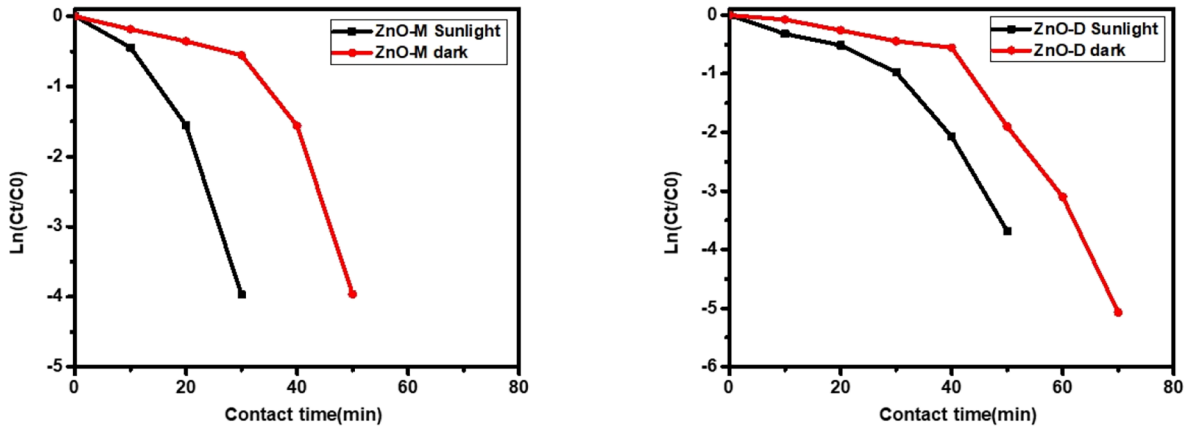

Figure 12. Results of $\ln(C_t/C_0)$ for the reduction of RhB dye by ZnO-M under dark/sunlight conditions and ZnO-D under dark/sunlight conditions.

Table 6. Degradation of RhB with ZnO-M and RhB Dye with ZnO-D

	RhB with ZnO-M		RhB dye with ZnO-D	
catalyst name	R^2	K_{app}	R^2	K_{app}
ZnO-M dark	0.81	6.8×10^{-1} min^{-1}	0.86	6.1×10^{-1} min^{-1}
ZnO-M sunlight	0.89	13.6×10^{-1} min^{-1}	0.91	6.8×10^{-1} min^{-1}

Table 7. Removal (%) of RhB with ZnO-M and RhB with ZnO-D

	RhB with ZnO-M		RhB with ZnO-D	
catalyst name	removal (%)	removal time (min)	removal (%)	removal time (min)
ZnO-M dark	98	50	96	70
ZnO-M sunlight	99	30	97	60

induced electron−hole pair generation, which accelerates the reaction. In the absence of sunlight (dark conditions), this energy source is absent, leading to slower reaction rates.

4. CONCLUSIONS

In this study, an efficient approach was developed to support ZnO NPs with the *W. coagulans* plant. ZnO NPs were prepared in both methods. The ZnO-D (aqueous solution) are more stable in water-based environments, minimizing agglomeration and phase changes. Conversely, ZnO NPs synthesized in methanol (ZnO-M) tend to perform better in organic solvents and nonaqueous settings. ZnO-M had greater control over particle size and morphology, potentially resulting in smaller, more uniform NPs. ZnO-D achieved fine size control but not potentially better than that compared to organic solvents. The choice should align with your application's stability requirements and desired particle size characteristics. The synthesized ZnO NPs were characterized by different advanced techniques, e.g., UV−vis, FTIR, SEM, XRD, DLS, and EDX. UV−vis spectroscopy gave a sharp peak for ZnO-D at 368.5 nm and at 354.5 nm for ZnO-M. The XRD spectra showed the wurtzite hexagonal structure of both samples of ZnO NPs based on the reported data. FESEM observed spherical shapes for ZnO-D NPs and flowering shapes for ZnO-M. The EDX and FTIR spectra are the same for both samples. The different phytochemical tests and antioxidant activity of the *W. coagulans* medicinal plant were estimated by TPC, TOC, TFC, and DPPH assay. The results indicated that the selected plant is a good natural source of antioxidants. In this study, water and methanolic extracts were used for the biosynthesis of ZnO NPs. ZnO NPs were found to be active in the degradation of RhB dye under sunlight. Furthermore, the antibacterial activity of ZnO NPs showed that the inhibition zone (mm) for ZnO-M is greater than ZnO-D against various pathogenic bacteria like *S. aureus* and *P. aeruginosa* and no inhibition zone was shown against *E. coli*. The antimicrobial properties of the biosynthesized NPs were also evaluated against a number of Gram-positive and Gram-negative pathogenic strains, which recommended that these could be used as substitute therapeutics against the drug-resistant microbes in the global emergence of drug resistance. It was concluded that the biosynthesized ZnO NPs of the methanolic extract have more potential against bacterial pathogens than ZnO-D and *W. coagulans*, which is a great natural source of antioxidants. The study opens doors to a range of future prospects in photocatalysis, biomedicine, nanotoxicology, and sustainable chemistry. Continued research and development in these areas may lead to innovative applications of *W. coagulans*-mediated ZnO NPs.

AUTHOR INFORMATION

Corresponding Authors

Saima Maher − *Department of Chemistry, Sardar Bahadur Khan Women University Quetta, Quetta 87300, Pakistan*; orcid.org/0000-0002-4269-6398; Email: saimamaher@yahoo.com

Muhammad Imran − *Department of Chemistry, Faculty of Science, King Khalid University, Abha 61413, Saudi Arabia*; Email: imranchemist@gmail.com

Authors

Bakht Zamina − *Department of Chemistry, Sardar Bahadur Khan Women University Quetta, Quetta 87300, Pakistan*

Musarat Riaz − *Department of Chemistry, Sardar Bahadur Khan Women University Quetta, Quetta 87300, Pakistan*

Sana Riaz − *Department of Botany, University of Karachi, Karachi 72500, Pakistan*

Noreen Khalid − *Faculty of Pharmacy, University of Sargodha, Sargodha, Punjab 40100, Pakistan*

https://doi.org/10.1021/acsomega.3c05947
ACS Omega 2023, 8, 46715−46727

Shagufta Fahmid − *Department of Chemistry and Department of Biotechnology, Sardar Bahadur Khan Women University Quetta, Quetta 87300, Pakistan*
Hina Ishtiaq − *Department of Biotechnology, Sardar Bahadur Khan Women University Quetta, Quetta 87300, Pakistan*
Shafia Parveen − *Department of Chemistry, Sardar Bahadur Khan Women University Quetta, Quetta 87300, Pakistan*

Complete contact information is available at:
https://pubs.acs.org/10.1021/acsomega.3c05947

Notes

The authors declare no competing financial interest.

■ ACKNOWLEDGMENTS

The authors express their appreciation to the Deanship of Scientific Research at King Khalid University, Saudi Arabia, for funding through research groups program under grant number R.G.P. 2/579/44.

■ REFERENCES

(1) Mulens-Arias, V.; Nicolas-Boluda, A.; Silva, A. K. A.; Gazeau, F. Theranostic iron oxide nanoparticle cargo defines extracellular vesicle-dependent modulation of macrophage activation and migratory behavior. *Adv. Biosyst.* **2018**, *2*, 1800079.
(2) Vo-Dinh, T.; *In: Nanotechnology in Biology and Medicine: Methods, Devices, and Applications*. Vo-Dinh, T, editor. CRC Press: Boca Raton, FL, 2nd ed., 2007.
(3) Maher, S.; Nisar, S.; Aslam, S. M.; Saleem, F.; Behlil, F.; Imran, M.; Assiri, M. A.; Nouroz, A.; Naheed, N.; Khan, Z. A.; Aslam, P. Synthesis and characterization of zno nanoparticles derived from biomass (sisymbrium irio) and assessment of potential anticancer activity. *ACS Omega* **2023**, *8*, 15920−15931.
(4) Monica, J. C.; Heintz, M. E.; Lewis, P. T. The perils of pre-emptive regulation. *Nat. Nanotechnol.* **2007**, *2*, 68−70.
(5) Albrecht, M. A.; Evans, C. W.; Raston, C. L. Green chemistry and the health implications of nanoparticles. *Green Chem.* **2006**, *8*, 417−432.
(6) Yoldas, B. E. Monolithic glass formation by chemical polymerization. *J. Mater. Sci.* **1979**, *14*, 1843−1849.
(7) Isley, S. L.; Penn, R. L. Titanium dioxide nanoparticles: effect of Sol−Gel pH on phase composition, particle size, and particle growth mechanism. *J. Phys. Chem. C* **2008**, *112*, 4469−4474.
(8) de Coelho Escobar, C.; dos Santos, J. H. Z. Effect of the sol-gel route on the textural characteristics of silica imprinted with Rhodamine B. *J. Sep. Sci.* **2014**, *37* (7), 868−875.
(9) Borm, P. J.; Robbins, D.; Haubold, S.; Kuhlbusch, T.; Fissan, H.; Donaldson, K.; Schins, R.; Stone, V.; Kreyling, W.; Lademann, J.; Krutmann, J.; Warheit, D.; Oberdorster, E. The potential risks of nanomaterials: A review carried out for ECETOC. *Particle Fibre Toxicol.* **2006**, *3*, 11−35.
(10) Ali, K.; Dwivedi, S.; Azam, A.; Saquib, Q.; Al-Said, M. S.; Alkhedhairy, A. A.; Musarrat, J. Aloe vera extract functionalized zinc oxide nanoparticles as nanoantibiotics. *J. Colloid Interface Sci.* **2016**, *472*, 145−156.
(11) Singh, P.; Kim, Y. J.; Zhang, D.; Yang, D. C. Biological Synthesis of Nanoparticles from Plants and Microorganisms. *Trends Biotechnol.* **2016**, *34*, 588−599.
(12) Jones, M. R.; Osberg, K. D.; Macfarlane, R. J.; Langille, M. R.; Mirkin, C. A. Templated techniques for the synthesis and assembly of plasmonic nanostructures. *Chem. Rev.* **2011**, *111* (6), 3736−3827.
(13) Matei, A.; Cernica, I.; Cadar, O.; Roman, C.; Schiopu, V. Synthesis and characterization of ZnO − polymer nanocomposites. *Int. J. Mater. Form.* **2008**, *1*, 767−770.
(14) Ghule, K.; Ghule, A. V.; Chen, B. J.; Ling, Y. C. Preparation and characterization of ZnO nanoparticles coated paper and its antibacterial activity study. *J. Green Chem.* **2006**, *8*, 1034−1041.
(15) Tam, K. H.; Djurišić, A. B.; Chan, C. M. N.; Xi, Y. Y.; Tse, C. W.; Leung, Y. H.; Chan, W. K.; Leung, F. C. C.; Au, D. W. T. Antibacterial activity of ZnO nanorods prepared by a hydrothermal method. *Thin Solid Films* **2008**, *516* (18), 6167−6174.
(16) Sawai, J. Quantitative evaluation of antibacterial activities of metallic oxide powders (ZnO, MgO and CaO) by conductimetric assay. *J. Microbiol. Methods* **2003**, *54* (2), 177−182.
(17) Slavin, Y. N.; Asnis, J.; Häfeli, U. O.; Bach, H. Metal nanoparticles: Understanding the mechanisms behind antibacterial activity. *J. Nanobiotechnol.* **2017**, *15*, 1−20.
(18) Wang, L.; Hu, C.; Shao, L. The antimicrobial activity of nanoparticles: Present situation and prospects for the future. *Int. J. Nanomed.* **2017**, *12*, 1227−1249.
(19) Al-Dhabi, A. N.; Arasu, V. M. Environmentally-Friendly Green Approach for the Production of Zinc Oxide Nanoparticles and Their Anti-Fungal, Ovicidal, and Larvicidal Properties. *Nanomaterials* **2018**, *8* (7), 500.
(20) Ali, A.; Maher, S.; Khan, A. S.; Chaudhary, I. M.; Musharraf, G. S. Sensitive quantification of six steroidal lactones in *Withania coagulans* extract by UHPLC electrospray tandem mass spectrometry. *Steroids.* **2015**, *104*, 176−181.
(21) Maher, S.; Choudhary, M. I.; Saleem, F.; Rasheed, S.; Waheed, I.; Halim, S. A.; Azeem, M.; Abdullah, I. B.; Froeyen, M.; Mirza, M. U.; Ahmad, S. Isolation of Antidiabetic Withanolides from *Withania coagulans* Dunal and Their In Vitro and In Silico Validation. *Biology* **2020**, *9* (8), 197.
(22) Hasan, M.; Zafar, A.; Yousaf, M.; Gulzar, H.; Mehmood, K.; Hassan, S. G.; Saeed, A.; Yousaf, A.; Mazher, A.; Rongji, D.; Mahmood, N. Synthesis of loureirin B-loaded nanoliposomes for pharmacokinetics in rat plasma. *ACS Omega.* **2019**, *4*, 6914−6922.
(23) Al-Dhabi, A. N.; Arasu, V. M. Environmentally-Friendly Green Approach for the Production of Zinc Oxide Nanoparticles and Their Anti-Fungal, Ovicidal, and Larvicidal Properties. *Nanomaterials* **2018**, *8* (7), 500.
(24) Elango, G.; Roopan, S. M.; Dhamodaran, K. I.; Elumalai, K.; Al-Dhabi, N. A.; Arasu, M. V. Spectroscopic investigation of biosynthesized nickel nanoparticles and its larvicidal, pesticidal activities. *J. Photochem. Photobiol. B* **2016**, *162*, 162−167.
(25) Fakhari, S.; Jamzad, M.; Kabiri, H. F. Green synthesis of zinc oxide nanoparticles: a comparison. *Green Chem. Lett. Rev.* **2019**, *12* (1), 19−24.
(26) Harborne, J. B.; *Phytochemical Methods*; Chapman and Hall Ltd.: London 1973, 49−188 DOI: 10.1007/978-94-009-5921-7.
(27) Obadoni, B. O.; Ochuko, P. O. Phytochemical Studies and Comparative Efficacy of the Crude Extract of Some Homeostatic Plants in Edo and Delta States of Nigeria. *Global J. of Pure Appl. Sci.* **2002**, *8*, 203−208.
(28) Kamath, D. S.; Arunkumar, D.; Avinash, G. N.; Samshuddin, S. Determination of total phenolic content and total antioxidant activity in locally consumed food stuffs in Moodbidri, Karnataka, India. *Adv. Appl. Sci. Res.* **2015**, *6* (6), 99−102.
(29) Barku, A. Y. V.; Opoku-Boahen, Y.; Owusu-Ansah, E.; Mensah, E. F. Antioxidant Activity and the Estimation of Total Phenolic and Flavonoid Contents of the Root Extract of Amaranthus spinosus. *Asian J. Plant Sci. Res.* **2013**, *3* (69), 13.
(30) Saleem, F.; Mehmood, R.; Mehar, S.; Khan, M. T. J.; Khan, Z.-U.-D.; Ashraf, M.; Ali, M. S.; Abdullah, I.; Froeyen, M.; Mirza, M. U.; Ahmad, S. Bioassay Directed Isolation, Biological Evaluation and in Silico Studies of New Isolates from Pteris cretica L. *Antioxidants* **2019**, *8* (7), 231.
(31) Mehar, S.; Ali, I.; Sami, A.; Ismail, M.; Naheed, N.; Khan, A. S.; Ahmed, V. U. Screening of Some Medicinal Plants for Antibacterial Activityagainst Conjunctivitiss. *J. Anim. Plant Sci.* **2017**, *27* (6), 2069−2074.
(32) Smoluchowski, M. V. "Versuch einer mathematischen Theorie der Koagulationskinetik kolloider Lösungen" ("Attempt at a Mathematical Theory of the Coagulation Kinetics of Colloidal Solutions"). *Z. Phys. Chem.* **1921**, *92*, 129−168.

(33) Li, X.; Xu, H.; Chen, Z.-S.; Chen, G. Biosynthesis of Nanoparticles by Microorganisms and Their Applications. Nanostructures for Medicine and Pharmaceuticals. *J. Nanomater.* **2011**, *2011*, 270974 DOI: 10.1155/2011/270974.
(34) Anitha, R.; Ramesh, K. V.; Ravishankar, T. N.; Sudheer Kumar, K. H.; Ramakrishnappa, T. Cytotoxicity, antibacterial and antifungal activities of ZnO nanoparticles prepared by the *Artocarpus gomezianus* fruit mediated facile green combustion method. *J. Sci. Adv. Mater. Devices* **2018**, 3, 440−451.
(35) Lundstedt, E.; Kahne, D.; Ruiz, N. Assembly and maintenance of lipids at the bacterial outer membrane. *Chem. Rev.* **2021**, *121*, 5098−5123.
(36) Dorobantu, L. S.; Fallone, C.; Noble, A. J.; Veinot, J.; Ma, G.; Goss, G. G.; Burrell, R. E. Toxicity of Silver Nanoparticles against Bacteria, Yeast, and Algae. *J. Nanopart. Res.* **2015**, *17*, 172.
(37) Tamayo, L.; Azócar, M.; Kogan, M.; Riveros, A.; Páez, M. Copper-Polymer Nanocomposites: An Excellent and Cost-Effective Biocide for Use on Antibacterial Surfaces. *Mater. Sci. Eng. C* **2016**, *69*, 1391−1409.
(38) Loraine, G.; Chahine, G.; Hsiao, C.; Choi, J.; Aley, P. Disinfection of gram-negative and gram-positive bacteria using DYNAJETS hydrodynamic cavitating jets. *Ultrason. Sonochem.* **2012**, *19*, 710−717.
(39) Espitia, P. J. P.; Soares, N. d. F. F.; Coimbra, J. S. d. R.; de Andrade, N. J.; Cruz, R. S.; Medeiros, E. A. A. Zinc oxide nanoparticles: Synthesis, antimicrobial activity and food packaging applications. *Food Bioprocess Technol.* **2012**, *5*, 1447−1464.
(40) Duffus, J. H. Heavy metals-a meaningless term? *Pure Appl. Chem.* **2002**, *74* (5), 793−807.
(41) Qi, P.; Lin, Z.; Li, J.; Wang, C.; Meng, W.; Hong, H.; Zhang, X. Development of a rapid, simple and sensitive HPLC-FLD method for determination of rhodamine B in chili-containing products. *Food Chem.* **2014**, *164*, 98−103.
(42) Mohammed Ali, H. S. H.; Sumiya; Anwar, Y.; Al-Ghamdi, Y. O.; Fakieh, M.; Khan, S. A. Revealing the Effect of MnO2, Activated Carbon and MnO2 /Activated Carbon on Chitosan Polymer Host Fabricated CoNPs: Antibacterial Performance and Degradation of Organic Compounds. *Polymers* **2022**, *14*, 627.
(43) Riaz, M.; Khan, N.; Khan, S. A.; Saeeduddin; Ahmad, Z.; Khan, M. A.; Iqbal, M.; Hemeg, H. A.; Bakhsh, E. M.; Khan, S. B. Enhanced catalytic reduction/degradation of organic pollutants and antimicrobial activity with metallic nanoparticles immobilized on copolymer modified with NaY zeolite films. *J. Mol. Liq.* **2022**, *359*, No. 119246.
(44) Byrappa, K.; Subramani, A. K.; Ananda, S.; Rai, K. M. L.; Dinesh, R.; Yoshimura, M. Photocatalytic degradation of rhodamine B dye using hydrothermally synthesized ZnO. *Bull. Mater. Sci.* **2006**, *29*, 433−438.
(45) Al Hamedi, F. H.; Rauf, M. A.; Ashraf, S. S. Degradation studies of Rhodamine B in the presence of UV/H_2O_2. *Desalination* **2009**, *239*, 159−166.

https://doi.org/10.1021/acsomega.3c05947
ACS Omega 2023, 8, 46715−46727